Eur. Phys. J. C (2017) 77:56
DOI 10.1140/epjc/s10052-017-4626-y

THE EUROPEAN PHYSICAL JOURNAL C

Regular Article - Theoretical Physics

Single-diffractive Drell–Yan pair production at the LHC

Federico Alberto Ceccopieri[1,2,a]

[1] Dipartimento di Fisica e Geologia, Università degli Studi di Perugia, INFN, Sezione di Perugia, Perugia, Italy
[2] IFPA, Université de Liège, 4000 Liège, Belgium

Received: 25 August 2016 / Accepted: 16 January 2017 / Published online: 28 January 2017

Abstract We present predictions for single-diffractive low-mass Drell–Yan pair production in pp collisions at the LHC at $\sqrt{s} = 13$ TeV. Predictions are obtained adopting a factorised form for the relevant cross sections and are based on a new set of diffractive parton distributions resulting from the QCD analysis of combined HERA leading proton data. We discuss a number of observables useful to characterise the expected factorisation breaking effects.

1 Introduction

The diffractive physics program pursued at the HERA ep collider in the recent past has substantially improved our knowledge on the dynamics of this class of processes. In the deep inelastic regime, the presence of a hard scale enables the derivation of a dedicated factorisation theorem [1–4] which allows the investigation of the partonic structure of the colour singlet exchanged in the t-channel. From scaling violations of the diffractive Deep Inelastic Scattering (DDIS) structure functions, quite precise diffractive parton distributions functions (dPDFs) have been extracted by performing QCD analysis [5–8] of available data.

With this tool available, factorisation tests have been conducted in order to investigate the range of validity of this hypothesis in processes other than DDIS. Factorisation has been shown to hold, as expected theoretically, in diffractive dijets production in DIS, where NLO predictions based on dPDFs well describe experimental cross sections [6,9] both in shape and normalisation. Factorisation breaking effects are expected to appear in diffractive photoproduction of dijets due to the resolved component of the quasi-real photon. In such a case, however, H1 [9] reported a global suppression factor of data over NLO theory around 0.5 while ZEUS [10] found the same ratio compatible with unity. To date, these conflicting results prevent to draw a conclusive statement about factorisation in this case. We note, however, that the measurements of diffractive dijet photoproduction in ultra-peripheral collisions in pp and pA collisions at the LHC [11] may offer an alternative way to settle this issue.

Complementary informations on the nature of diffraction has been provided by hard diffraction measurements in hadronic collisions. As theoretically anticipated in Refs. [1–3,12,13] and experimentally observed in $p\bar{p}$ collisions at Tevatron [14–16], factorisation is strongly violated in such a case. In particular, predictions based on a factorised expressions for the relevant cross sections in terms of diffractive parton distributions extracted from HERA data overestimate hard diffraction measurements by a factor $\mathcal{O}(10)$ [17]. This conclusion persists even after the inclusion of higher order QCD corrections [18].

A rich program at the LHC is being pursued in diffractive physics by all Collaborations either based on the identification of large rapidity gaps (LRG) [19–24] or by using dedicated proton spectrometers [25,26]. Complementing Tevatron ($\sqrt{s} = 1.96$ TeV) results with forthcoming ones from the LHC at higher centre-of-mass energies ($\sqrt{s} = 8, 13$ TeV) will give information on the energy dependence, if any, of the suppression factor, the so called rapidity gap survival (RGS) probability. Hopefully, they will allow to study its kinematic dependences, among which the one on the scale characterising the hard process appears to be particularly relevant. In the simplest scenario, it will be possible to clarify whether factorisation may still hold but revisited in a weak form through a global or local rescaling of diffractive PDFs extracted from DDIS and to study their degree of universality among different hard processes in hadronic collisions.

The purpose of the present paper is to present predictions for the single-diffractive Drell–Yan pair production at the LHC at $\sqrt{s} = 13$ TeV, one of the clean and simple measurable process in hadronic collisions. In such a process, the invariant mass of the lepton pair can easily be reconstructed and, depending on experimental capabilities, pushed to rather low values, allowing a detailed characterisation of the hard-

[a] e-mail: federico.alberto.ceccopieri@cern.ch

scale dependence of the suppression factor. Although estimates of the latter are present in the literature for the specific process at hand [27–29], we take a conservative approach and avoid to introduce any suppression factor. We further assume factorisation to hold and adopt factorised expressions for the relevant cross sections. A preliminary set of, newly generated, diffractive parton distributions extracted from combined leading proton HERA data will be used for the calculation. In view of the expected factorisation breaking effects in hard, single-diffractive, measurements in hadronic collisions, the obtained values for the cross sections should be considered as upper bounds.

Given the exploratory nature of the analysis, more intended as a feasibility study, theoretical predictions are calculated to leading order accuracy. We take into account, however, the virtual photon decay into leptons so that cross sections can be studied as a function of, measurable, final state leptons kinematics. This allows us to explore the phase space available for the process and to estimate the impact of typical experimental cuts on the transverse momenta and rapidities of the leptons.

From QCD analyses performed in DDIS and anticipating the results of the next section, we know that the colour singlet exchanged in the t-channel is a gluon-enriched state. Since gluonic contributions to Drell–Yan production starts to $\mathcal{O}(\alpha_s)$ in perturbation theory, an accurate estimation of the suppression factor will require the inclusion of higher order corrections. The impact of the latter and a detailed report on the extraction of diffractive parton distributions to NLO accuracy will be presented in a companion publication.

The paper is organised as follows. In Sect. 2 we report in some details the extraction of diffractive PDFs from combined HERA leading proton data. In Sect. 3, making use of such distributions, we present results for single-diffractive Drell–Yan production in pp collisions at the LHC at $\sqrt{s} =$ 13 TeV. In Sect. 4 we summarise our results.

2 FIT overview

Diffractive DIS belongs to the Semi-Inclusive lepton–proton DIS process of the type

$$l(k) + p(P) \to l(k') + p(P') + X(p_X), \tag{1}$$

where, along with the outgoing lepton, an additional proton p is detected in the final state. In Eq. (1) X stands for the unobserved part of the hadronic final state and we indicate particles four-momenta in parentheses. In the lp centre-of-mass system, diffractive DIS events are then characterised by outgoing protons with a large momentum fraction of the incident proton and quite small values of the transverse momentum measured with respect to the collision axis, i.e. in the target fragmentation region of the incident proton. The kinematic variables used to describe the DIS process are the conventional Lorentz invariants

$$Q^2 = -q^2, \quad x_B = \frac{Q^2}{2P\cdot q}, \quad y = \frac{P\cdot q}{P\cdot k}, \tag{2}$$

with $q = k - k'$. Final state protons are instead described by the fractional momentum of the singlet exchange with respect to the proton momentum, $x_{I\!P}$, and the invariant momentum transfer t at the proton vertex:

$$x_{I\!P} = \frac{q\cdot(P-P')}{P\cdot q}, \quad t = (P-P')^2, \tag{3}$$

where typical DDIS selection requires $x_{I\!P} \lesssim 0.1$ and $|t| \lesssim 1$ GeV^2. In the following we will use the scaled fractional momentum variable β defined by $\beta = x_B/x_{I\!P}$. This is interpreted as the fractional momentum of interacting parton with respect to pomeron fractional momentum $x_{I\!P}$. The data are often presented in terms of the reduced lp cross section, $\sigma_r^{D(4)}$, which depends on the diffractive transverse and longitudinal structure functions $F_2^{D(4)}$ and $F_L^{D(4)}$, respectively. In the one-photon exchange approximation, it reads

$$\sigma_r^{D(4)}(\beta, Q^2, x_{I\!P}, t) = F_2^{D(4)}(\beta, Q^2, x_{I\!P}, t) - \frac{y^2}{1+(1-y)^2} F_L^{D(4)}(\beta, Q^2, x_{I\!P}, t). \tag{4}$$

According to the factorisation theorem [1–4], structure functions appearing in Eq. (4), are factorised into perturbatively calculable short-distance cross sections and diffractive parton distributions

$$F_k^{D(4)}(\beta, Q^2, x_{I\!P}, t) = \sum_i \int_\beta^1 \frac{\mathrm{d}\xi}{\xi} f_{i/p}^D(\beta, \mu_F^2; x_{I\!P}, t)\, C_{ki}\left(\frac{\beta}{\xi}, \frac{Q^2}{\mu_F^2}, \alpha_s(\mu_R^2)\right) + \mathcal{O}\left(\frac{1}{Q^2}\right). \tag{5}$$

The index i runs on the flavour of the interacting parton. The hard-scattering coefficients C_{ki} ($k = 2, L$) are perturbatively calculable as a power expansion in the strong coupling α_s and depend upon μ_F^2 and μ_R^2, the factorisation and renormalisation scales, respectively. The C_{ki} coefficient functions are the same as in fully inclusive DIS. Diffractive PDFs $f_{i/p}^D(\beta, \mu_F^2, x_{I\!P}, t)$ appearing in Eq. (5) are proton-to-proton fracture functions [30] in the very forward kinematical limit and can be interpreted as the number density of interacting partons at a scale μ_F^2 and fractional momentum β conditional to the detection of a final state proton with fractional momentum $1 - x_{I\!P}$ and invariant momentum transfer t. The t-unintegrated diffractive PDFs appearing in Eq. (5) obey standard DGLAP [31–33] evolution equations [34]. The same statement holds when they are integrated over t in a limited range [35]:

$$f^D_{i/p}(\beta, Q^2, x_{I\!P}) = \int_{t_{\min}}^{t_{\max}} \mathrm{d}t\, f^D_{i/p}(\beta, Q^2, x_{I\!P}, t), \quad t_{\max} \ll Q^2. \tag{6}$$

In this paper we analyse the combined H1 and ZEUS diffractive DIS cross sections measurements [36] of the process in Eq. (1) where leading protons are measured by dedicated forward spectrometers. The centre-of-mass energy for the e^+p scattering is $\sqrt{s} = 318$ GeV. This data set covers the phase space region $2.5 < Q^2 < 200$ GeV^2 and $0.0018 < \beta < 0.816$ and it has widest coverage in the proton fractional energy loss, $0.00035 < x_{I\!P} < 0.09$, subdivided in 10 bins in $x_{I\!P}$, with an average of 20 points per-$x_{I\!P}$ bin for a total of 192 points. At variance with all other DDIS cross sections measurements, the squared four-momentum transfer at the proton vertex, t, is integrated in the restricted range $0.09 < |t| < 0.55$ GeV^2 in order to minimise systematic uncertainties originating from t-extrapolation of the various measurements outside their respective measured ranges. The reduced cross sections in Eq. (4) are integrated over t in such a range and the diffractive PDFs in Eq. (6) are defined accordingly. For $x_{I\!P} < 0.03$ the data set overlaps with high-statistics LRG data set and for $0.03 < x_{I\!P} < 0.09$ it provides the best experimental information available on diffractive DIS cross sections. The combination procedure, in general, allows a reduction of the systematic uncertainties via cross-calibration of the various measurements. The direct detection of the forward proton allows one to avoid any systematics associated with the large rapidity gap selection. By definition, these data are free from the proton dissociative background which has been found to contribute around 23% of the diffractive DIS cross sections based on LRG selection [5]. Therefore this set of data provides the most precise knowledge about the absolute normalisation of diffractive DIS cross sections. These advantages, however, come at the price of increased uncertainties relative to LRG data given the reduced statistics of the sample. Diffractive parton distributions extracted form this data set will be used in the context of single hard diffraction in hadronic collisions in conjunction with ordinary parton distributions. In order to avoid any mismatch between inclusive and diffractive PDFs we adopt leading order CTEQL1 parton distribution set [37] evolved in the zero-mass variable-flavour-number scheme (ZM-VFNS). The evolution of diffractive PDFs is performed within the same scheme and to the same accuracy by using `QCDNUM17` [38] program. The QCD parameters are the ones quoted in Ref. [37]. In particular we set the charm and bottom masses to $m_c = 1.3$ GeV and $m_b = 4.5$ GeV, respectively, and the strong coupling is evaluated at one loop setting $\alpha_s^{n_F=5}(M_Z^2) = 0.130$. In general factorisation theorem [1–4] for diffractive DIS in the form of Eq. (5) holds at fixed values of $x_{I\!P}$ and t so that the parton content of the colour-singlet exchange described by f_i^D is uniquely controlled by the kinematics of the outgoing proton. Therefore, at least in principle, dPDFs may differ at different values of $x_{I\!P}$ and t. This idea has been successfully tested [7] in the analysis of LRG data from Ref. [5]. In the present context, given the limited number and accuracy of the data points in each $x_{I\!P}$ bin, we use a simpler approach, namely a fully factorised $\beta - x_{I\!P}$ ansatz for the flavour-symmetric singlet and gluon diffractive parton (momentum) distributions defined at the initial scale Q_0^2:

$$\begin{aligned} &\mathcal{F}(x_{I\!P}) = x_{I\!P}^{f_0}\ (1 + f_1 x_{I\!P}^{f_2}), \\ &\beta\Sigma(\beta, Q_0^2, x_{I\!P}) = \mathcal{F}(x_{I\!P})\ A_q\ \beta^{B_q}\ (1-\beta)^{C_q}(1 + D_q\beta^{E_q}), \\ &\beta g(\beta, Q_0^2, x_{I\!P}) = \mathcal{F}(x_{I\!P}) A_g\ \beta^{B_g}\ (1-\beta)^{C_g}. \end{aligned} \tag{7}$$

The initial conditions in Eq. (7) are characterised by a common flux factor $\mathcal{F}(x_{I\!P})$ controlled by a single power at low $x_{I\!P}$. An extra modulation, controlled by parameters f_1 and f_2, is introduced to accommodate the data at larger values of $x_{I\!P}$. In order to guarantee the vanishing of the singlet distribution on the endpoint, we fix the large-β behaviour of the singlet by setting $C_q = 0.5$ but additional freedom at intermediate values of β is allowed leaving D_q and E_q parameters free in the minimisation. Since the gluon distributions is only indirectly fixed by the slope of the reduced cross section, the gluon parameters B_g and C_g are highly correlated and we decide to fix $C_g = 0.5$ for a total of 9 free parameters. Such distributions, once evolved, are used to calculate the diffractive structure functions $F^D_{2,L}$ with the help of the `QCDNUM17` convolution engine and to reconstruct the diffractive reduced cross sections in Eq. (4) which are then minimised against data [36] with the help of the `MINUIT` [39] program. The choice of Q_0^2 is optimised performing a scan giving the best χ^2 value for $Q_0^2 = 1.5$ GeV^2. By using total errors quoted in the experimental analysis and the standard χ^2 definition, we obtain a total $\chi^2/d.o.f. = 0.913$. We report in Table 1 the best parameters and the breakdown of the contributions to χ^2 function in each $x_{I\!P}$ bin. According to these numbers there is no misrepresentation of the data across the $x_{I\!P}$ bins. The comparison of the best-fit results and the reduced cross sections is presented in Fig. 1 for four representative values of $x_{I\!P}$ as a function of Q^2 or β. We supplement the best-fit parametrisations with an additional set of parametrisations obtained according to the Hessian method outlined in Refs. [40,41] which allows the experimental uncertainties to propagate to arbitrary observables. We note that our initial conditions assume a common β-shape for the diffractive PDF in all $x_{I\!P}$ bins.

This theoretical hypothesis, in turn, determines an unrealistic precise determination of the diffractive PDFs if associated with the standard $\Delta\chi^2 = 1$ criterion, often exceeding the precision of the data. In order to correct for such an effect and to obtain a more conservative error estimate

Table 1 Left: Best-fit parameters. Right: Breakdown of χ^2 contributions in each $x_{I\!P}$ bin

Parameter	$p_i \pm \delta p_i$	$x_{I\!P}$	χ^2	Fitted points
f_0	-1.208 ± 0.022	0.00035	4.44	4
f_1	48.2 ± 11.9	0.0009	6.78	10
f_2	1.42 ± 0.13	0.0025	21.36	16
A_q	0.0039 ± 0.0007	0.0085	20.34	24
B_q	-0.237 ± 0.026	0.0160	20.70	26
C_q	0.5	0.0250	27.24	25
D_q	22.6 ± 2.8	0.0350	13.85	24
E_q	2.28 ± 0.20	0.0500	28.69	27
A_g	0.057 ± 0.011	0.0750	13.10	26
B_g	0.41 ± 0.13	0.0900	10.51	10
C_g	0.5	Total	167.0	192

we choose a tolerance criterion $\Delta\chi^2 = 10$ (one unit for $x_{I\!P}$ bin) and dPDFs alternative parametrisations are obtained with this choice. We have checked by explicit evaluation that each parametrisation gives a consistent value for the χ^2 function, $\chi^2_{\text{best}} + \Delta\chi^2$. The error bands presented in the plots are obtained according to this criterion. In Fig. 2 we present the singlet and gluon momentum distributions in two $x_{I\!P}$ bins at different scales. The singlet shows a bump in the large β region ($\beta \gtrsim 0.5$) at the lower scale which is progressively washed away by evolution at higher scales. The rise of the gluon distribution at small β is accelerated by pQCD evolution and it is the dominant contribution for $\beta \lesssim 0.1$.

We have further performed two consistency checks detailed below. The first one concerns the diffractive longitudinal structure function which contributes starting from $\mathcal{O}(\alpha_s)$ and it is absent to the accuracy of the present calculation. Since its dominant contributions appear in the large-y region, the fit

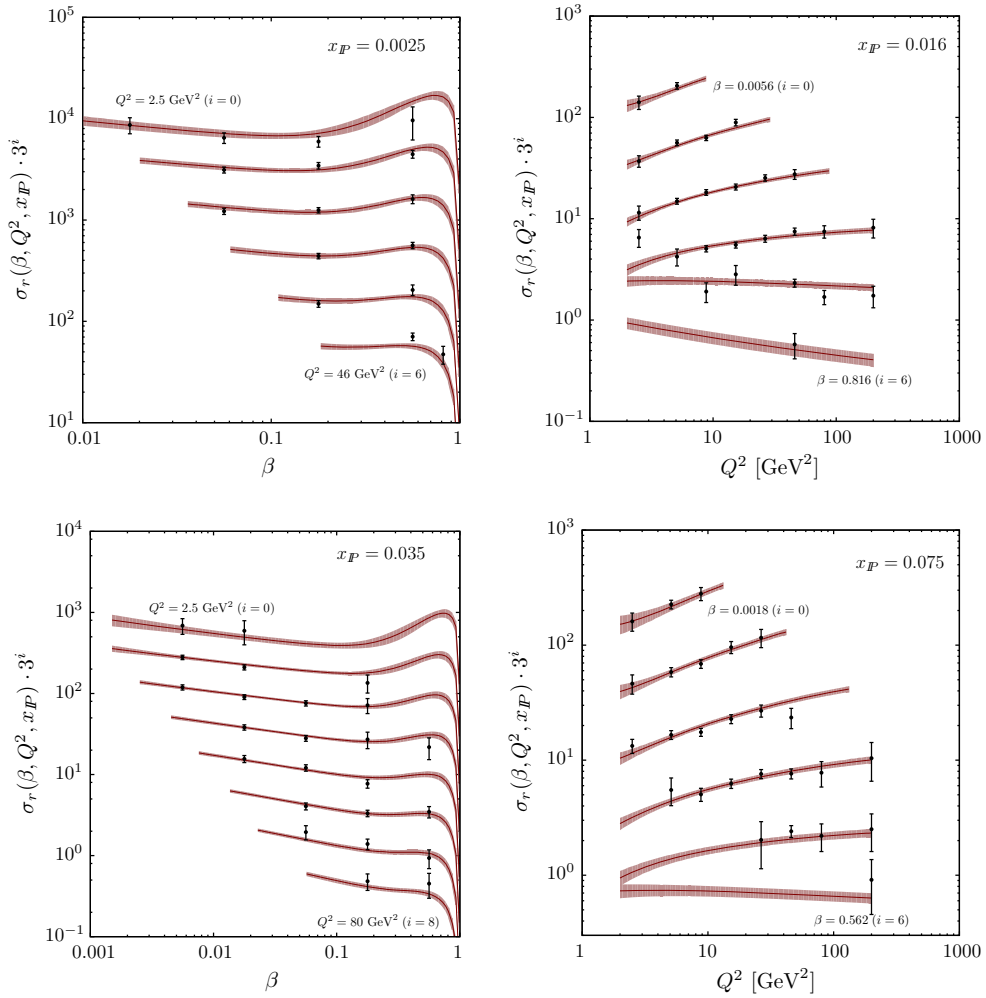

Fig. 1 Best-fit results compared to combined H1-ZEUS data [36]. The reduced cross section as a function as a function of β or Q^2 is displayed in four representative bins of $x_{I\!P}$. *Error bars* are total uncertainties. The band represents the propagation of experimental uncertainties according to the $\Delta^2_\chi = 10$ criterion, as discussed in the text

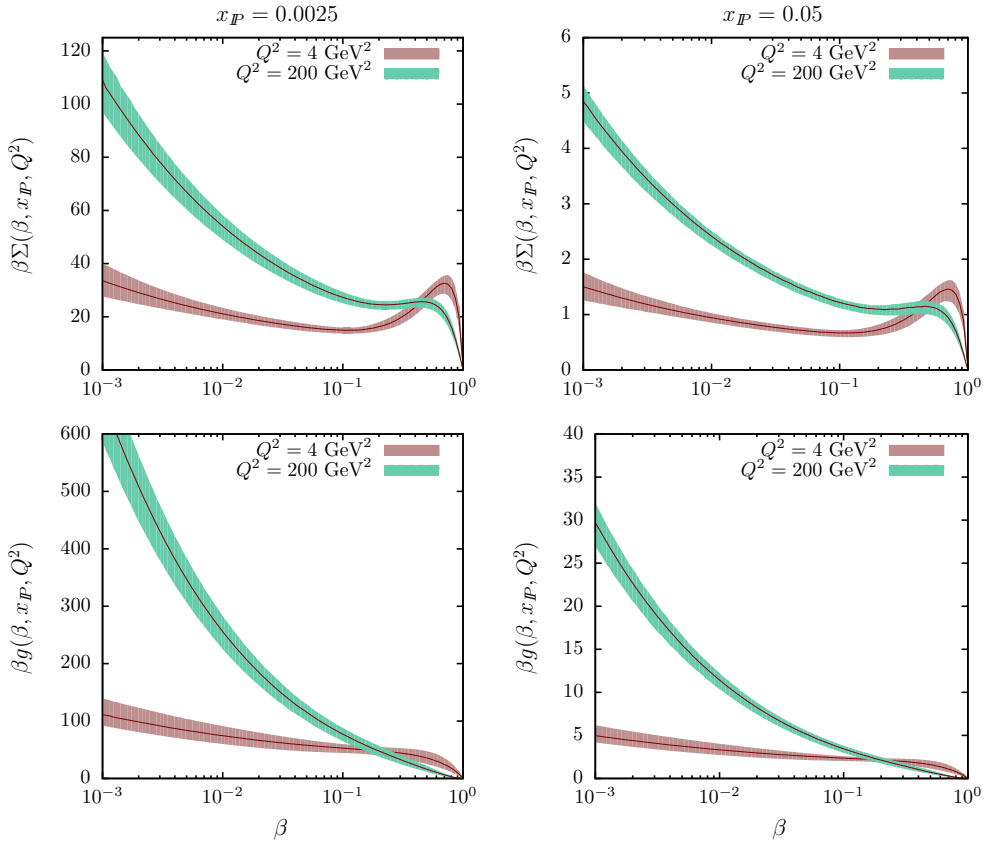

Fig. 2 Diffractive parton distributions from best-fit evolved for two values of Q^2 and $x_{I\!P}$ as a function of β. The *band* represents the propagation of experimental uncertainties according to the $\Delta^2_\chi = 10$ criterion, as discussed in the text

has been repeated with the cut $y < 0.5$ imposed. The second one addresses the issue, reported in previous analyses [5–8], of the inclusion in the fit of the lowest Q^2 points. For such a reason, the minimisation has been repeated by including only data points for which $Q^2 > 6\,\text{GeV}^2$. In both cases we observe a modest decrease in the $\chi^2/d.o.f$. However, as shown in Fig. 3, the resulting parametrisations are compatible, within uncertainties, with the ones obtained without imposing the cuts. Given the substantial stability of the results against variation of the phase space boundary of data included in the fit, we consider the "no cut" scenario as our default choice and use the corresponding best-fit parametrisations in the next section.

We conclude this section presenting a comparison between dPDFs obtained in this work with the ones already present in the literature. In Fig. 4 we compare our dPDFs with LO Fit B (without error estimation) and NLO Fit B (with error estimation) parametrisations presented in Ref. [5] and obtained from DDIS data selected with the large rapidity gap method. Since the analysis presented in Ref. [5] excludes DDIS data for which $Q^2 < 8.5\,\text{GeV}^2$, the comparison is performed at the higher scale $Q^2 = 25\,\text{GeV}^2$, a value for which no extrapolation is required. The normalisation of dPDFs extracted in Ref. [5] is larger than the one of the present analysis given the larger t-range, $|t| < 1\,\text{GeV}^2$, used in Ref. [5] to define the DDIS cross sections. A further upward normalisation shift is generated by the proton dissociative contribution which amounts to 23% of the DDIS cross section measured with the large rapidity gap method [5] and it is absent in the present analysis. In the left panel of Fig. 4, the comparison is performed at $x_{I\!P} = 0.0025$ where both data sets overlap. In this case, the larger data sample in this $x_{I\!P}$-bin used in the fit of Ref. [5] induce smaller experimental uncertainties (yellow band) on dPDFs with respect to the ones presented in this work. The virtue of the present parametrisations can be better appreciated for $x_{I\!P} > 0.03$, being the latter the maximal $x_{I\!P}$-value included in the analysis of Ref. [5]. In the right panel of Fig. 4, the comparison is therefore performed at $x_{I\!P} = 0.05$. Diffractive PDFs from Ref. [5] are in a full extrapolation range and we observe a substantial increase of their uncertainties (green error band) driven by the theoretical errors associated with the parametrisations of the flux factor at large $x_{I\!P}$. On the contrary, our parametrisations, despite the lower statistical power of the data set used in this analysis, show a much reduced error. To conclude, we note that the singlet distribution from Ref. [5]

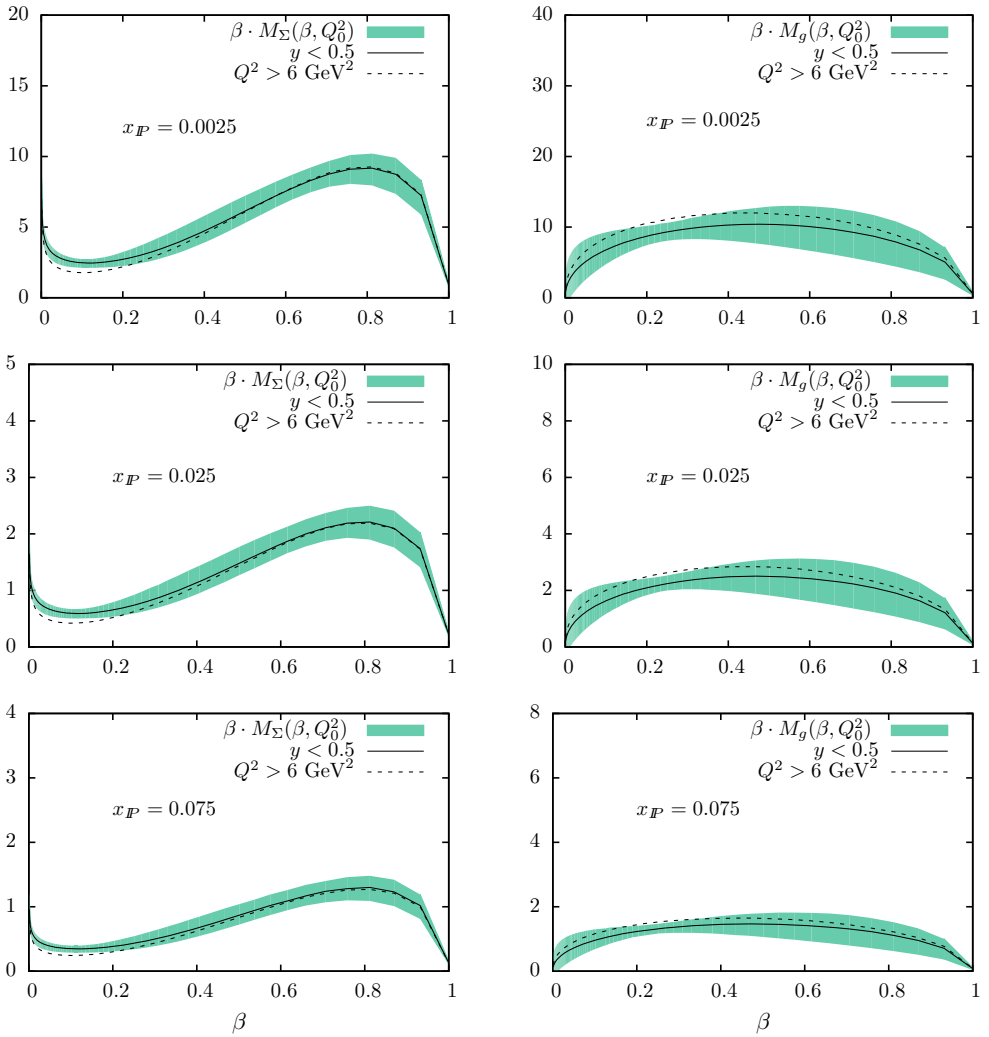

Fig. 3 Diffractive singlet (*left*) and gluon (*right*) momentum distributions at $Q_0^2 = 1.5$ GeV^2 for different values of $x_{I\!P}$. Best-fit distributions with uncertainties (the band corresponds to $\Delta\chi^2 = 10$) are compared with parametrisations returned by the fit with the cut $y < 0.5$ (*solid*) or $Q^2 > 6$ GeV^2 (*dashed*) imposed

is stable in shape and normalisation between the LO and NLO versions and shows the presence of a large-β bump in nearly the same position with respect to the one obtained in the present analysis. On the contrary we observe a steeper behaviour of the LO FitB gluon with respect to the NLO FitB one and to the one from our fits. This is probably due to the fixed flavour number scheme used in Ref. [5] which, by construction, induces a larger gluon distribution with respect to the one obtained with a variable-flavour-number scheme.

3 Single-diffractive Drell–Yan production

The signature of hard diffraction in hadronic collisions is the presence of hard-scattering process associated with the production of a leading proton. Among many others, we consider here the simplest hard-scattering process, namely the Drell–Yan pair production. Therefore we consider the reaction

$$p(P_1) + p(P_2) \to p(P) + \gamma^*(\to l^+(p_3) + l^-(p_4)) + X. \tag{8}$$

The invariant mass of the pair $q^2 = (p_3 + p_4)^2 = Q^2$ is chosen to be large enough so that perturbative QCD can be applied. In hadronic collisions, the Lorentz-invariant variable z is used to characterise final state hadrons and is defined by

$$z = \frac{2P \cdot (P_1 + P_2)}{s} \equiv \frac{2E_p^*}{\sqrt{s}} \equiv 1 - x_{I\!P}. \tag{9}$$

In the hadronic centre-of-mass frame, where the second identity holds, z is just the observed proton energy, E_p^*, scaled down by the beam energy, $\sqrt{s}/2$. Hard diffractive events are

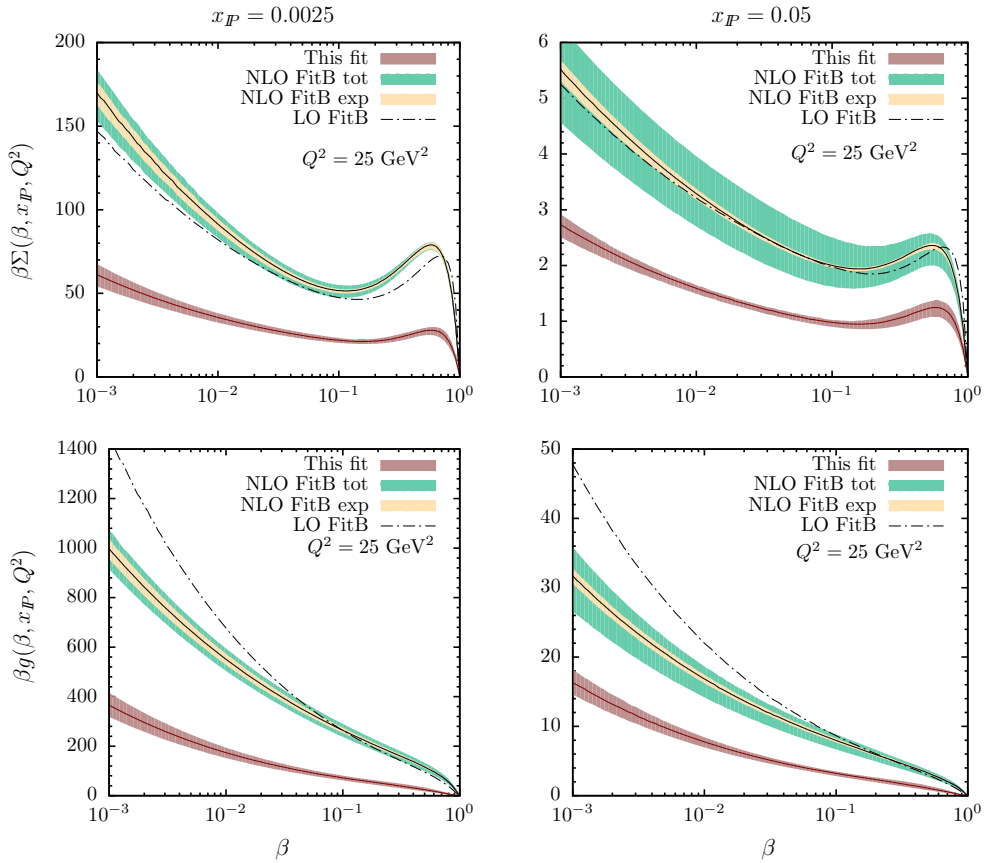

Fig. 4 Diffractive singlet and gluon momentum distributions as a function of β for two values of $x_{I\!P}$ at $Q^2 = 25$ GeV^2 compared to LO and NLO Fit B parametrisations of Ref. [5], with the latter supplemented with experimental (*yellow band*) and experimental plus theoretical errors added in quadrature (*green band*)

then characterised by low values of the invariant $x_{I\!P}$ and t, both in the same range of values as the one measured in DDIS.

In Eq. (8), we assume that the proton with momentum P_1 is moving in the $+z$ direction and the leading proton with momentum P is produced quasi-collinearly to P_1 at large and positive rapidities. At the cross section level, diffractive parton distributions for the proton with momentum P_1 will be used. The same process, of course, may occur also in the opposite emisphere and, since the hadronic initial state is symmetric, will be not considered here.

At the partonic level and to lowest order in the strong coupling, the process proceeds via the annihilation of a quark–antiquark pair into a massive virtual photon which subsequently decays into a opposite-sign lepton pair. To be definite we consider here the decay into muons:

$$q(p_1) + \bar{q}(p_2) \to \mu^+(p_3) + \mu^-(p_4). \tag{10}$$

Before discussing our results we found useful to sketch some details of the calculation. The incoming parton momenta in the hadronic centre-of-mass-system are given by

$$p_1 = x_1 \frac{\sqrt{s}}{2}(1, 0_\perp, 1), \quad p_2 = x_2 \frac{\sqrt{s}}{2}(1, 0_\perp, -1), \tag{11}$$

with $s = (P_1 + P_2)^2$. We choose as final state variables the lepton rapidities y_3, y_4, and lepton transverse momentum, $\boldsymbol{p_t}$. In terms of the latter, the four-momenta of the leptons are given by

$$p_3^\mu = (p_t \cosh y_3, \boldsymbol{p_t}, p_t \sinh y_3), \tag{12}$$
$$p_4^\mu = (p_t \cosh y_4, -\boldsymbol{p_t}, p_t \sinh y_4), \tag{13}$$
$$q^\mu = (M \cosh Y, \boldsymbol{0}, M \sinh Y), \tag{14}$$

with $p_t = |\boldsymbol{p_t}|$ and $q = p_3 + p_4$. Assuming factorisation to hold, the differential cross section, to leading order accuracy, involves appropriate products of diffractive and ordinary parton distributions functions. It reads

$$\frac{\mathrm{d}\sigma^D}{\mathrm{d}y_3 \mathrm{d}y_4 \mathrm{d}p_t \mathrm{d}x_{I\!P}} = \sum_q e_q^2 \frac{f_q^D(\beta, x_{I\!P}, \mu_F^2)}{x_{I\!P}} \times f_{\bar{q}}(x_2, \mu_F^2) \frac{2p_t\hat{s}}{3s} \frac{2\pi\alpha_{em}^2}{\hat{s}^2} \frac{\hat{t}^2 + \hat{u}^2}{\hat{s}^2}, \tag{15}$$

where the sum runs over quark and antiquarks. In actual calculations we have set the factorisation scale to $\mu_F = M_{\mu\mu}$. We further introduce the leptons rapidity sum, Y, and difference $\bar{y}$:

$$Y = \frac{1}{2}(y_3 + y_4), \quad \bar{y} = \frac{1}{2}(y_3 - y_4). \tag{16}$$

The former defines the rapidity of the virtual photon. The partonic Mandelstam invariants appearing in Eq. (15) are then given by

Table 2 Outline of the muon-pair and proton phase space regions and the corresponding fiducial cross section for single-diffractive Drell–Yan pair production, $\sigma^{SD,DY}$, with associated experimental and theoretical errors

$pp \to \mu^+\mu^-\ p\ X$	$\sqrt{s} = 13$ TeV
Muon-pair kinematics	$\lvert y^\mu \rvert < 2.45$
	$2 < \mathrm{M}_{\mu\mu} < 20$ GeV
	No cuts on muon p_t or $\boldsymbol{p}$
Proton kinematics	$0.09 < \lvert t \rvert < 0.55$ GeV^2
	$10^{-4} < x_{I\!P} < 10^{-1}$
$\sigma^{SD,DY}$	1635 ± 60 (exp) $^{+670}_{-460}$ (scale) pb

$$\hat{s} = p_t^2(e^{\bar{y}} + e^{-\bar{y}})^2 \equiv M_{\mu\mu}^2, \tag{17}$$

$$\hat{t} = (p_1 - p_3)^2 = -p_t^2(1 + e^{-2\bar{y}}), \tag{18}$$

$$\hat{u} = (p_1 - p_4)^2 = -p_t^2(1 + e^{2\bar{y}}). \tag{19}$$

In terms of these variables the momentum fractions are given by

$$\beta = \frac{x_1}{x_{I\!P}} = \frac{p_t}{x_{I\!P}\sqrt{s}}(e^{y_3} + e^{y_4}) \equiv \frac{M_{\mu\mu}}{x_{I\!P}\sqrt{s}}e^{Y}, \tag{20}$$

$$x_2 = \frac{p_t}{\sqrt{s}}(e^{-y_3} + e^{-y_4}) \equiv \frac{M_{\mu\mu}}{\sqrt{s}}e^{-Y}. \tag{21}$$

Since the two momentum fractions cannot exceed unity, the following bounds can be derived:

$$\ln\sqrt{\tau} < Y < \ln x_{I\!P} - \ln\sqrt{\tau}, \tag{22}$$

with $\tau = M_{\mu\mu}/\sqrt{s}$. Given the kinematic constraint $x_1 \leqslant x_{I\!P}$, the pair rapidity spans an increasingly asymmetric range as $x_{I\!P}$ decreases. For $x_{I\!P} < \sqrt{\tau}$, the pair is entirely in the $Y < 0$ rapidity range. Formally, the rapidity range for the inclusive Drell–Yan case is recovered simply setting $x_{I\!P} = 1$ in Eq. (22).

In the present analysis we focus on diffractive processes tagged with dedicated instrumentation [25,26]. We choose

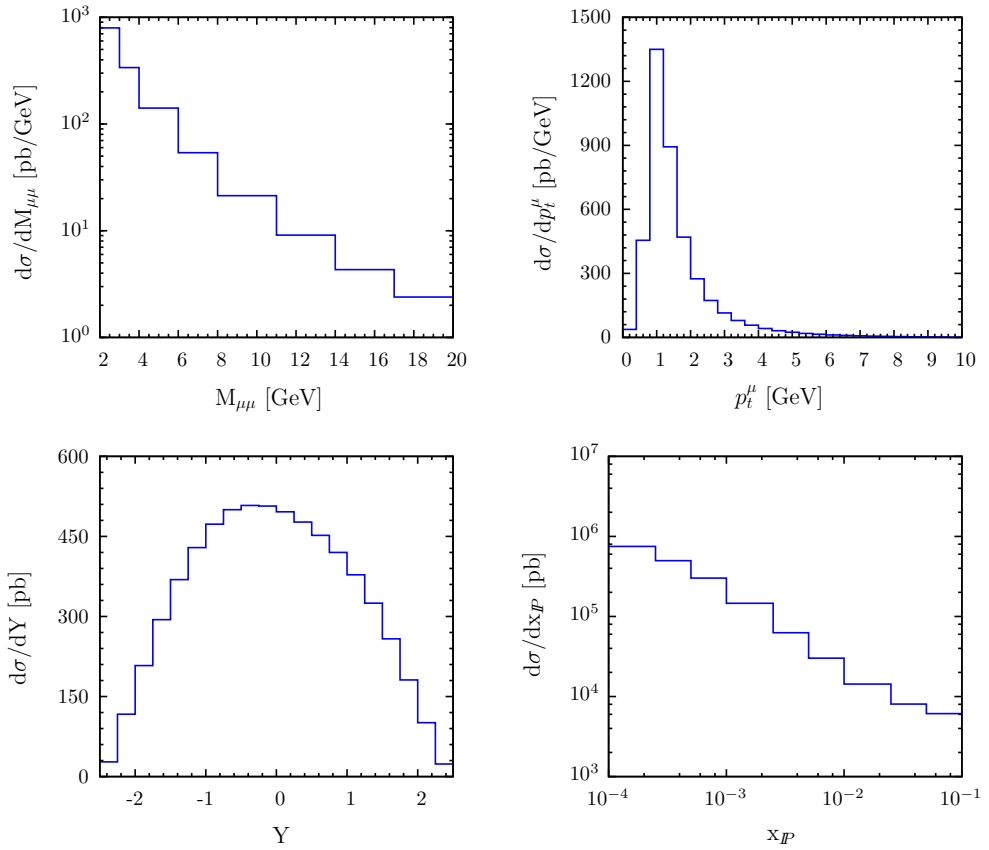

Fig. 5 Single-diffractive Drell–Yan production. *Top left* Invariant-mass distribution. *Top right* Transverse momentum distribution of final state muons. *Bottom left* Muon-pair-rapidity distribution. *Bottom right* $x_{I\!P}$ distribution

the proton fractional momentum loss to be in the range $10^{-4} < x_{I\!P} < 10^{-1}$, with maximal overlap with the range measured at HERA [36]. Predictions presented in the following are integrated over the t-range of the data [36] out of which dPDFs are estracted, i.e. $0.09 < |t| < 0.55\ \mathrm{GeV}^2$. We set the centre-of-mass energy of the pp collisions to $\sqrt{s} = 13$ TeV. The invariant mass of the muon pair is required to be in the range $2 < \mathrm{M}_{\mu\mu} < 20$ GeV, a range of virtualities in line with those measured at HERA. We assume that the J/Ψ and Υ contributions, which both lie within this mass range, can be properly subtracted from the data sample. We require both muons to have rapidity $|y^{\mu}| < 2.45$ but we do not apply cuts either on the muons transverse or three momenta.

The resulting fiducial cross sections for single-diffractive Drell–Yan pair production is reported in Table 2. In the case that proton spectrometers are installed on both sides of the interaction point, such a result for the fiducial cross section should be doubled. As already anticipated, the quoted result does not include any rapidity gap suppression factor and predictions refer to virtual photon decay in the muon channel. The first error represents the propagation of experimental uncertainties as obtained in the diffractive PDF fit. The second one, of theoretical nature, is obtained varying the factorisation scale μ_F^2 appearing in both distributions in Eq. (15) in the range $1/2M_{\mu\mu}^2 < \mu_F^2 < 2M_{\mu\mu}^2$. In this regime of relatively low Q^2 values where diffractive and inclusive parton distributions evolve faster, we find that the dominant error source, of theoretical nature, is associated with missing higher order corrections. The latter are known to high accuracy for a number of distributions and will be considered in a separate publication. In the present contest, predictions can be stabilised against factorisation scale variation by considering appropriate ratios of diffractive over inclusive cross sections. This issue will be discussed in some details at the end of this section. We begin our overview of predictions showing in Fig. 5 single-differential cross sections in the fiducial phase space region specified in Table 2. The pair invariant-mass distribution is shown in the top left panel and rapidly falls as an inverse power of $\hat{s} = M_{\mu\mu}^2$ typical of annihilation processes into massive states, as it can be read out from

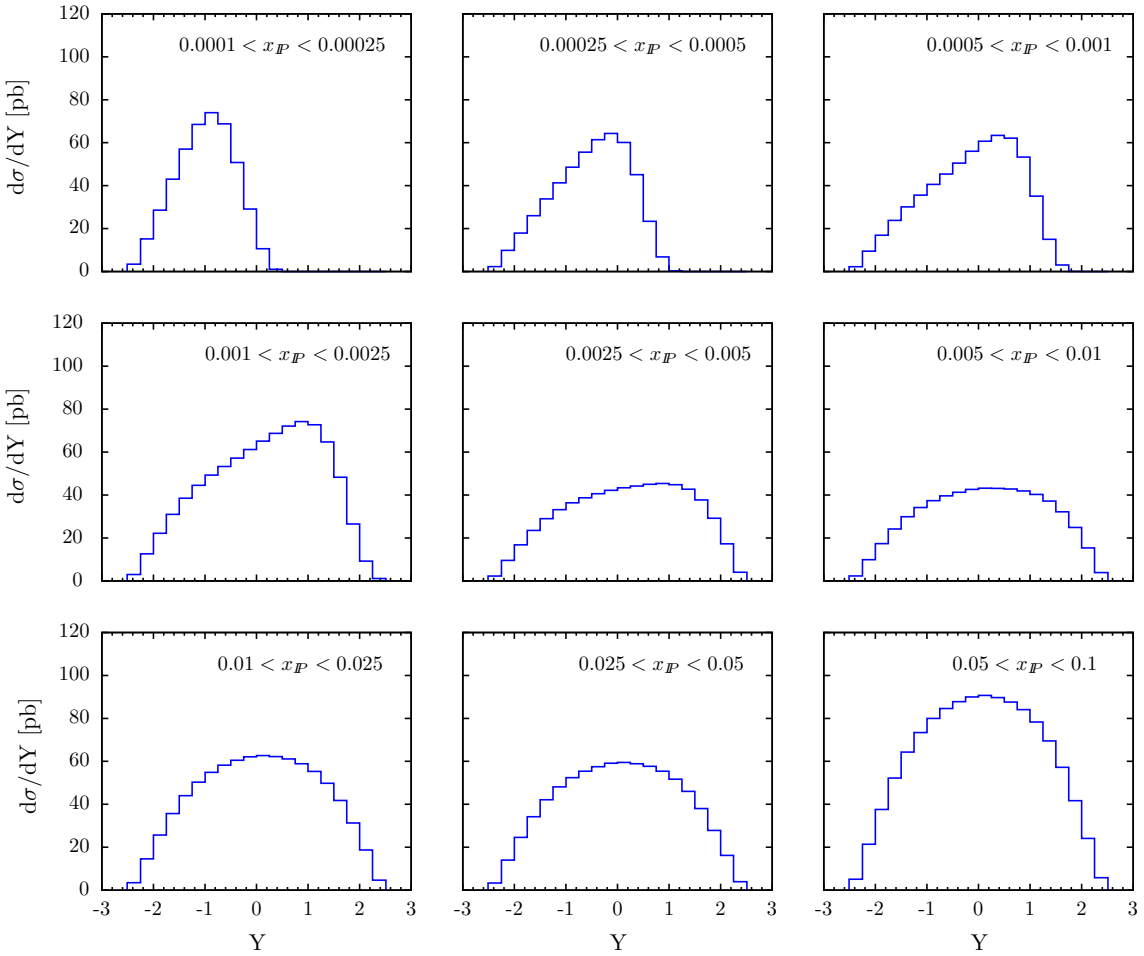

Fig. 6 Muon-pair-rapidity distribution in bins of $x_{I\!P}$ integrated over the fiducial range $2 < M_{\mu\mu} < 20$ GeV

Eq. (15). In the top right panel the muon transverse momentum distribution is presented. Its kinematically allowed range extends up to $p_t = M_{\mu\mu}^{\max}/2$. Given the fast falling nature of the $M_{\mu\mu}$-distribution, dominated by low values of the invariant, the muon transverse momentum distribution shows a maximum (the Jacobian peak) at $p_t = M_{\mu\mu}^{\min}/2$. The muon-pair-rapidity distribution, presented in the bottom left panel, is slightly asymmetric and indicates a preference for the virtual photon to populate the negative rapidity hemisphere (the one containing the dissociated proton, in the chosen reference frame). We note that, despite phase space limitations introduced by Eq. (22) and the difference between diffractive and ordinary parton distributions, the muon pair populates the available rapidity range, as defined by the muon rapidity cuts and by Eq. (16). In the bottom right panel we present the $x_{I\!P}$ distribution. In general, it is well known that such distribution behaves approximately as an inverse power of $x_{I\!P}$ at small $x_{I\!P}$. In the present case, the flattening of the distribution at small $x_{I\!P}$ can be ascribed to the shrinkage of phase space for the production of massive pair, since the maximum partonic centre-of-mass energy is reduced to $\sqrt{x_{I\!P}s}$. The kinematic of the scattered proton induces peculiar features on muon-pair production whose effects are presented in Fig. 6 in terms of the muon-pair rapidity, Y, in various bins of $x_{I\!P}$. The distributions is strongly asymmetric at the lowest values of $x_{I\!P}$, where the muon pair populates the negative rapidity range (dissociated proton direction) due to the kinematic constraint $x_1 < x_{I\!P}$. In the intermediate $x_{I\!P}$ range the pair starts to populate the positive emisphere (diffractive proton direction) with a tendency to show a maximum in this range. At even higher values of $x_{I\!P}$, the available centre-of-mass for the reaction increases and the distribution progressively turns into a symmetric one. Given the relatively light masses produced, this regime is sensitive to parton distributions evaluated at relatively small values of β and x_2, the symmetry of the rapidity distribution indicates that the shapes of the sea component of the diffractive and ordinary distributions are similar, both being driven by QCD evolution. This complicated pattern is further illustrated in Fig. 7 where the single-differential cross section as a function of Y is shown in four different ranges of the pair invariant mass and integrated over $x_{I\!P}$. In all mass bins, the distributions show a maximum in the negative rapidity range, a signal that the interacting parton from the dissociated proton carries, on average, slightly more momentum with respect to the one originating from the scattered proton. In Fig. 8 we present single-differential distributions as a function of $x_{I\!P}$ in four different invariant-mass ranges. As the invariant mass increases, we observe a progressive flattening

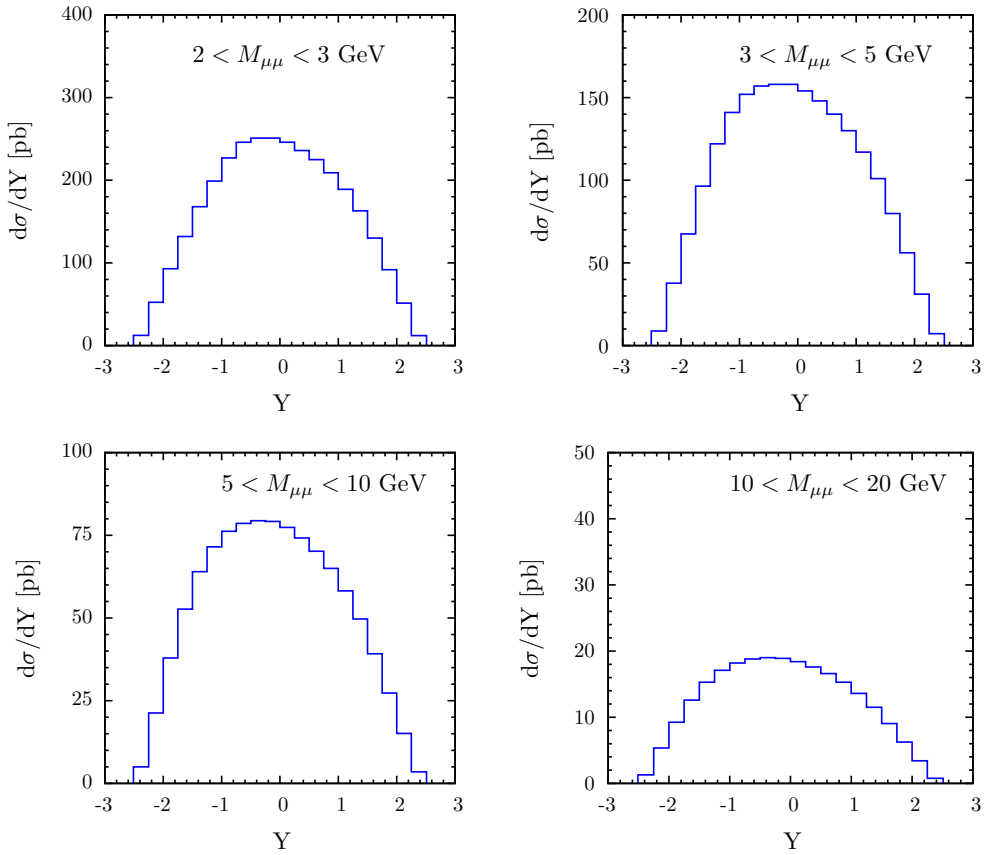

Fig. 7 Single-diffractive Drell–Yan production. Muon-pair-rapidity distribution in bins of $M_{\mu\mu}$

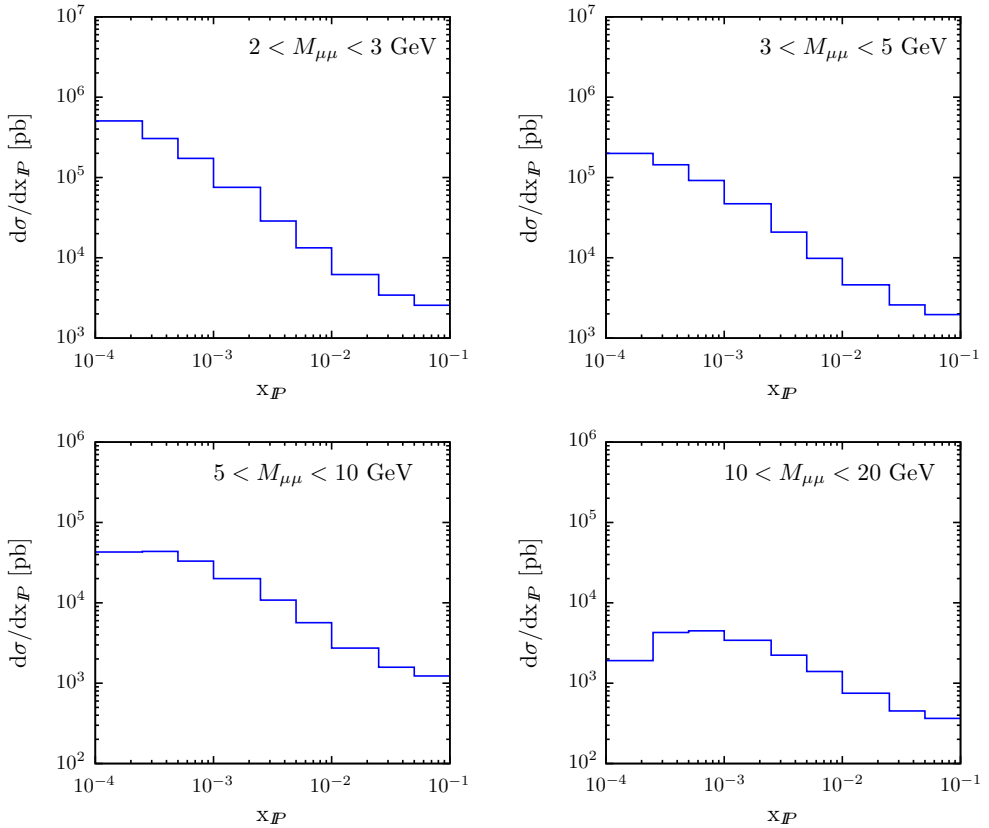

Fig. 8 Single-diffractive Drell–Yan production. Drell–Yan $x_{I\!P}$-distribution in four mass ranges

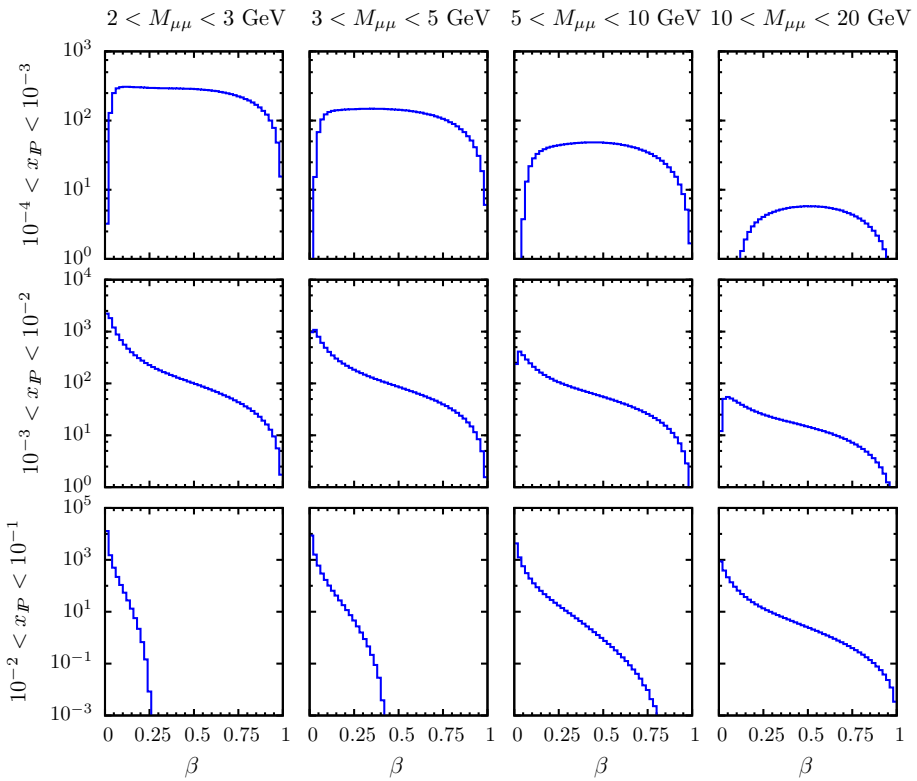

Fig. 9 Single-diffractive Drell–Yan production. β-distribution in bins of $M_{\mu\mu}$ and $x_{I\!P}$

of the distributions at small $x_{I\!P}$. This effect is due to the phase space reduction induced by the constraint $M^2_{\mu\mu} = \beta x_{I\!P} x_2 s$, which at low $x_{I\!P}$ disfavours the production of increasingly massive pair. In Fig. 9 we present single-differential cross section as a function of β, the fractional momentum of the interacting parton with respect to the one of the colour singlet exchanged in the t-channel, integrated in various bins of $M_{\mu\mu}$ and $x_{I\!P}$. Such distributions offer insight in the sensitivity of the cross section to diffractive parton distributions, modulo kinematics effects. In the lowest $x_{I\!P}$ bin the distributions span all the allowed β range and progressively shrinks at large β as $x_{I\!P}$ increases, a natural consequence of momentum conservation. As already shown in Figs. 6 and 9, the distributions in the pair rapidity Y are asymmetric around $Y = 0$. The asymmetry decreases both as the mass of the pair increases and as $x_{I\!P}$ increases. Such an effect is absent in the inclusive Drell–Yan case initiated by a symmetric initial state. This effect is better appreciated considering the absolute and relative asymmetries, A_a and A_r, respectively, defined by

$$A_a(Y) = \frac{\mathrm{d}\sigma(Y) - \mathrm{d}\sigma(-Y)}{\sigma^{SD,DY}},$$
$$A_r(Y) = \frac{\mathrm{d}\sigma(Y) - \mathrm{d}\sigma(-Y)}{\mathrm{d}\sigma(Y) + \mathrm{d}\sigma(-Y)}. \tag{23}$$

They differ by a different normalisation and are shown in the left panel of Fig. 10 along with the associated theoretical errors estimated via factorisation scale variations. The absolute asymmetry, integrated over all masses and proton energy loss, reaches its maximum 3% at $Y \simeq 1$ and is always negative, implying that the muon pair is produced mostly in the hemisphere opposite to the one containing the scattered proton. The relative asymmetry shows an even more pronounced behaviour. Since for $Y \to 0$ the rapidity distribution becomes symmetric and the cross section is maximal, see the bottom left panel of Fig. 5, the asymmetry vanishes and the corresponding error band shrinks in that limit. Both asymmetries, being normalised to single-diffractive cross sections, are not affected by uncertainties due to the rapidity gap survival factor. They are primarily sensitive to the shape of diffractive PDFs and show reasonably stability against scale variations. Depending on the accumulated integrated luminosity, this predicted behaviour, absent in the inclusive case, could be exploited to correlate the forward proton detection with the central Drell–Yan production. As discussed at the beginning of the section, predictions are affected by large theoretical errors associated with scale variations. Such uncertainties can be conveniently reduced by considering the ratio R of diffractive to inclusive cross sections

$$R = \frac{\sigma(pp \to pXY)}{\sigma(pp \to XY)}, \tag{24}$$

which also offers the advantage reducing the experimental systematics errors. In Eq. (24) Y stands for the selected hard-scattering process (Drell–Yan in this case) and X for the unobserved part of the final state. At Tevatron the ratio R has been measured in a variety of final state [14–16] and it shows a quite stable behaviour with a value close to 1%. For the single-diffractive Drell–Yan production in pp collisions at $\sqrt{s} = 13$ TeV, the ratio R is presented in the right panel of Fig. 10. Given our leading order estimate of the inclusive Drell–Yan cross section, R varies between 6 and 8%

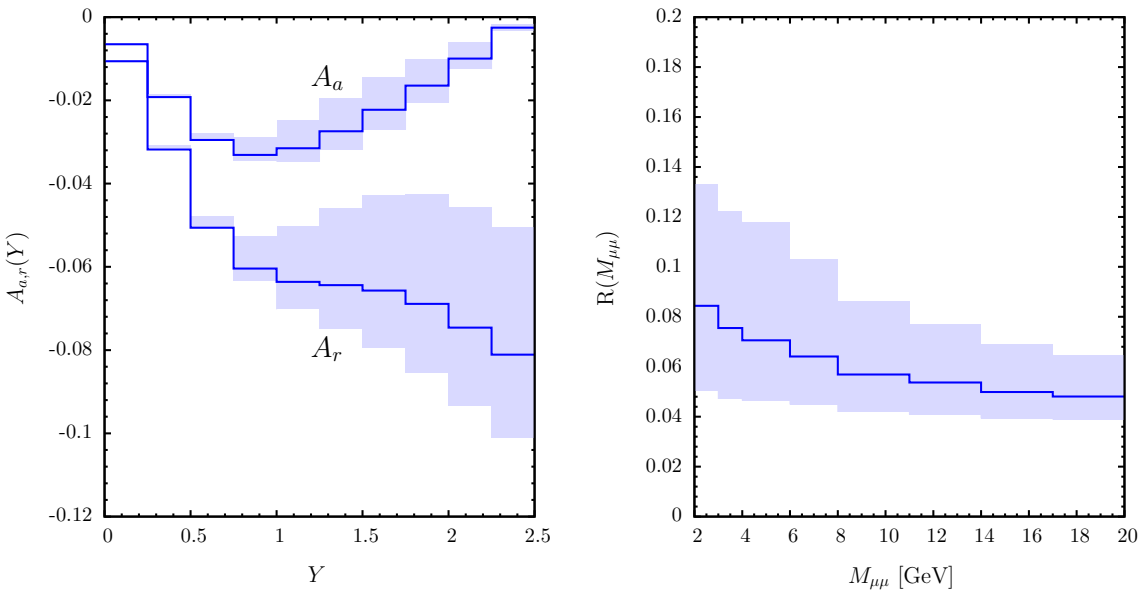

Fig. 10 *Left panel* Asymmetry of the pair-rapidity distribution. *Right panel* Ratio of diffractive over inclusive Drell–Yan cross sections as a function of the muons' invariant mass, $M_{\mu\mu}$. The *light-blue bands* represent the theoretical errors associated to factorisation scale variations

and decreases mildly as a function of the invariant mass of the pair, $M_{\mu\mu}$. This prediction, however, does not take into account the RGS suppression factor. In this respect it would be interesting to check whether the data follow at least the shape of the ratio as a function of $M_{\mu\mu}$.

4 Conclusions

In this paper we have considered the single-diffractive production of low-mass Drell–Yan pair in pp collisions at the LHC at $\sqrt{s} = 13$ TeV. Predictions are based on a fully factorised approach for the cross section which makes use of a set of diffractive parton distributions obtained from a QCD fit to combined leading proton DIS data from HERA. A number of distributions are presented both in terms of Drell–Yan pair and scattered proton variables. Examples of asymmetries and ratio are constructed in order to minimise theoretical and experimental uncertainties. In view of the foreseen measurements of this type of process at the LHC Run-II, these results constitute a baseline for the characterisation of the expected factorisation breaking effects.

Acknowledgements This work is supported in part through the project "Hadron Physics at the LHC: looking for signatures of multiple parton interactions and quark gluon plasma formation (Gossip project)", funded by the "Fondo ricerca di base di Ateneo" of the Perugia University. We warmly thank Marta Ruspa for numerous discussions on the LHC measurements and for providing us details of the analysis presented in Ref. [36]. We also thank Sergio Scopetta for reading the manuscript before submission.

Funded by SCOAP[3].

References

1. J.C. Collins, Phys. Rev. D **57**, 3051 (1998)
2. J.C. Collins, Phys. Rev. D **61** (2000) 019902 (E)
3. J.C. Collins, J. Phys. G **28**, 1069 (2002)
4. M. Grazzini, L. Trentadue, G. Veneziano, Nucl. Phys. B **519**, 394 (1998)
5. H1 Collaboration (A. Aktas et al.), Eur. Phys. J. C **48**, 715 (2006)
6. ZEUS Collaboration (S. Chekanov et al.), Nucl. Phys. B **831**, 1 (2010)
7. F.A. Ceccopieri, L. Favart, e-Print: arXiv:1205.6356, arXiv:1110.4829
8. H1 Collaboration (A. Aktas et al.), JHEP **0710**, 042 (2007)
9. H1 Collaboration (V. Andreev et al.), JHEP **1503**, 092 (2015)
10. ZEUS Collaboration (S. Chekanov et al.), Eur. Phys. J. C **55**, 177 (2008)
11. V. Guzey, M. Klasen, JHEP **1604**, 158 (2016)
12. A. Berera, D.E. Soper, Phys. Rev. D **50**, 4328 (1994)
13. J.C. Collins et al., Phys. Lett. B **307**, 161 (1993)
14. C.D.F. Collaboration, T. Affolder et al. Phys. Rev. Lett. **84**, 232 (2000)
15. CDF Collaboration (T. Aaltonen et al.), Phys. Rev. D **86**, 032009 (2012)
16. CDF Collaboration (T. Aaltonen et al.), Phys. Rev. D **82**, 112004 (2010)
17. L. Alvero et al., Phys. Rev. D **59**, 074022 (1999)
18. M. Klasen, G. Kramer, Phys. Rev. D **80**, 074006 (2009)
19. ATLAS Collaboration (G. Aad et al.), Eur. Phys. J. C **72**, 1926 (2012)
20. CMS Collaboration (S. Chatrchyan et al.), Phys. Rev. D **87** 1, 012006 (2013)
21. CMS Collaboration (V. Khachatryan et al.), Phys. Rev. D **92** (2015) 1, 012003
22. CMS Collaboration (S. Chatrchyan et al.), Eur. Phys. J. C **72**, 1839 (2012)
23. ALICE Collaboration (B. Abelev et al.), Eur. Phys. J. C **73**, 6, 2456 (2013)
24. LHCb Collaboration (R. Aaij et al.), Eur. Phys. J. C **73**, 2421 (2013)
25. L. Adamczyk et al., Technical Report. ATLASTDR-024, CERN-LHCC-2015-009
26. M. Albrow et al., Technical Report. TOTEMTDR-003, CMS-TDR-13, CERN-LHCC-2014-021
27. R.S. Pasechnik, B.Z. Kopeliovich, I. Potashnikova, Phys. Rev. D **86**, 114039 (2012)
28. R.S. Pasechnik, B.Z. Kopeliovich, Eur. Phys. J. C **71**, 1827 (2011)
29. B.Z. Kopeliovich et al., Phys. Rev. D **74**, 114024 (2006)
30. L. Trentadue, G. Veneziano, Phys. Lett. B **323**, 201 (1994)
31. Yu.L. Dokshitzer, Sov. Phys. JETP **46**, 641 (1977)
32. V.N. Gribov, L.N. Lipatov, Sov. J. Nucl. Phys. **15**, 438 (1972)
33. G. Altarelli, G. Parisi, Nucl. Phys. B **126**, 298 (1977)
34. G. Camici, M. Grazzini, L. Trentadue, Phys. Lett. B **439**, 382 (1998)
35. F.A. Ceccopieri, L. Trentadue, Phys. Lett. B **655**, 15 (2007)
36. H1 and ZEUS Collaborations (F.D. Aaron et al.), Eur. Phys. J. C **72**, 2175 (2012)
37. J. Pumplin et al., JHEP **0207**, 012 (2002)
38. M. Botje, Comput. Phys. Commun. **182**, 490 (2011)
39. F. James et al., Comput. Phys. Commun. **10**, 343 (1975)
40. J. Pumplin et al., Phys. Rev. D **65**, 014013 (2001)
41. A.D. Martin et al., Eur. Phys. J. C **28**, 455 (2003)